ACS APPLIED MATERIALS & INTERFACES

Research Article

www.acsami.org

Optical Constants of Amorphous, Transparent Titanium-Doped Tungsten Oxide Thin Films

C. V. Ramana,* Gaurav Baghmar, Ernesto J. Rubio, and Manuel J. Hernandez

Department of Mechanical Engineering, University of Texas at El Paso, El Paso, Texas 79968, United States

ABSTRACT: We report on the optical constants and their dispersion profiles determined from spectroscopic ellipsometry (SE) analysis of the 20%-titanium (Ti) doped of tungsten oxide (WO_3) thin films grown by sputter-deposition. The Ti-doped WO_3 films grown in a wide range of temperatures (25−500 °C) are amorphous and optically transparent. SE data indicates that there is no significant interdiffusion at the film−substrate interface for a W−Ti oxide film growth of ~90 nm. The index refraction (n) at λ = 550 nm vary in the range of 2.17−2.31 with a gradual increase in growth temperature. A correlation between the growth conditions and optical constants is discussed.

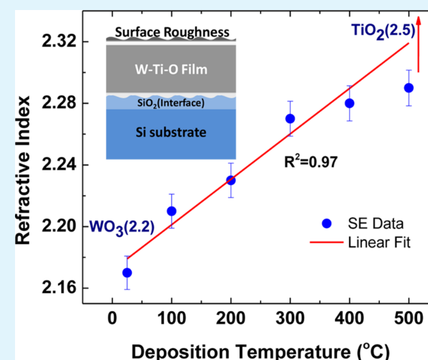

KEYWORDS: *tungsten oxide, Ti-doping, sputter-deposition, microstructure, optical constants*

I. INTRODUCTION

Tungsten oxide (WO_3) is an intensively studied "chromogenic" material because of the coloration effects associated with various processes.[1−6] There has been a great deal of recent interest in low-dimensional structures, such as nanorods, nanowires, nanoparticles and ultrathin films, of WO_3 for a wide variety of applications in optoelectronics, microelectronics, photovoltaic devices, selective catalysis, and environmental engineering.[2−40] WO_3 has been in use for the development of smart windows for energy-efficient architecture of buildings and automobiles, flat-panel displays, optical memory and writing−reading−erasing devices, and electronic information displays.[1−6] Most recently, WO_3 based materials are considered and demonstrated to be attractive for application in photoelectrochemical cells (PECs) for hydrogen production by water-splitting.[19−21] In addition, new application of WO_3 in emerging dye-sensitized solar cells (DSSC) technology has been demonstrated recently.[22] While the efficiency is not comparable to those employing the most studied TiO_2-based DSSCs, options to tailor the microstructure and chemistry in order to improve the efficiency exists.[22,23]

The optical, photochemical, and electrical properties of metal oxide thin films grown from either chemical or physical vapor deposition methods are sensitive to the physical and chemical characteristics, which in turn depend on the processing conditions and precursor materials.[2−40] For instance, the density of TiO_2, SiO_2 HfO_2 and ZrO_2 thin films was shown to be sensitive to the processing conditions and influence the index of refraction of resulting films greatly.[41−43] Furthermore, oxides differ in stoichiometry, depending on the preparation conditions, leading to substantial changes in the electronic properties.[2−43] From this point of view, a detailed understanding and control over the physical parameters and optical properties of pure or doped W-oxide based thin films is required in order to optimize performance for a given application. In this article, we investigate and report on the observed amorphization and optical constants of titanium (Ti) doped WO_3 films grown by reactive sputter-deposition under varying growth temperature.

The relevance and current interest in Ti-doped oxide materials is derived from the following considerations. Recently, it has been demonstrated in several cases that either Ti metal doping or capping will alter the electronic structure of the oxide in order to benefit the properties and device performance.[44−51] Enhancement in the electrical conductivity, luminescence, sensing ability, and photocatalytic performance are the benefits expected and/or reported in the literature under controlled Ti incorporation or TiO_2-coupling with other oxides.[44−53] It has been reported that the near band edge luminescence enhances 5 times when in Ti/ZnO nanorod heterostructures, where Ti is sputtered onto ZnO at 400 °C.[44] Surface diffusion of Ti with a effective reduction in surface defects is accounted for by the enhanced luminescence of Ti/ZnO nanorod heterostructures.[44] For the specific case of W−Ti−O materials, while TiO_2 is a well-studied photocatalyst, coupling TiO_2 with WO_3 can extend the optical absorption to the visible region to enhance the photocatalytic efficiency.[45−50] Recently, studies focused on the TiO_2−WO_3 system proved the enhanced photocatalytic performance of such materials.[45−51] It has been pointed out that the key will be the specific composition and associated effect on the electronic structure and band gap.[45−51] It has been demonstrated that W−Ti mixed oxides exhibit enhanced

Received: October 31, 2012
Accepted: April 9, 2013
Published: May 17, 2013

ACS Publications © 2013 American Chemical Society

selectivity and sensitivity to certain chemicals for their utilization in integrated sensors.[52,53] Most recently, we have demonstrated that the electrical conductivity of 5% Ti-doped WO_3 can be enhanced compared to that of pure WO_3 films.[54,55] Therefore, investigating the fundamental aspects of microstructure evolution and structure−property relationships in W−Ti−O films may provide opportunities to tailor the microstructure and optical properties of the materials for the desired application. Specifically, if high optical transparency and improved electrical conductivity is demonstrated, there is a possibility to realize the new set of materials based on W−Ti mixed oxides, which can serve as transparent conducting electrodes for application in emerging of solar cell and optoelectronics technology. The results obtained of the optical constants of Ti-doped amorphous, transparent WO_3 films are reported in this paper.

II. EXPERIMENTAL SECTION

A. Film Growth. Titanium (20%) doped WO_3 thin films were deposited onto silicon (Si) wafers and optical grade quartz substrates by radio frequency (rf) (13.56 MHz) magnetron sputtering. The Si(100) wafers and quartz substrates were cleaned by RCA and chemical cleaning, respectively, as reported elsewhere.[54−57] After cleaning, all the substrates were dried with nitrogen before introducing them into the vacuum chamber, which was initially evacuated to a base pressure of $\sim 10^{-6}$ Torr. A W−Ti ($W_{0.8}Ti_{0.2}$) alloy target (Plasmaterials Inc.) of 2 in. diameter and 99.95% purity was employed for reactive sputtering. The $W_{0.8}Ti_{0.2}$-target was placed on a 2-in. sputter gun, which was correspondingly placed at a distance of 8 cm from the substrate. A sputtering power of 40 W was initially applied to the target while introducing high-purity argon (Ar) into the chamber causing plasma ignition. Once ignited, the power was increased to 100 W, and oxygen (O_2) was released into the chamber for reactive deposition. The flow of the Ar and O_2 and their ratio was controlled using MKS mass flow meters. Before each deposition, the $W_{0.8}Ti_{0.2}$-target was presputtered for 10 min using Ar alone with the shutter above the gun closed. The samples were deposited at different temperatures (T_s) varying from RT to 500 °C. The substrates were heated by halogen lamps, and the desired temperature was controlled by an Athena X25 controller. The deposition was made for 1 h duration to obtain a film thickness of ∼90 nm. The film thickness was verified with various analytical methods to ensure that films are with a reasonably constant thickness for comparison of the data and analysis presented and to understand the effect of growth temperature on the structure and properties.

B. Characterization. The grown Ti-doped WO_3 films were characterized by performing structural and optical measurements. X-ray diffraction (XRD) measurements on the samples grown on Si(100) were performed by using a Bruker D8 Advance X-ray diffractometer. In order to avoid interference by the substrate and obtain diffraction pattern of the coatings, grazing incidence X-ray diffraction (GIXRD) was performed on the films. All the measurements were made ex-situ as a function of T_s. GIXRD patterns were recorded using Cu Kα radiation (λ = 1.540 56 Å) at RT. A high voltage of 40 kV was used to generate the X-rays. The GIXRD patterns were recorded employing the X-ray beam fixed at a grazing incidence of 1°. The scanning was performed in a 2θ range of 15−70° using the "detector scan" mode, where the detector was independently moved in the plane of incidence to collect the diffraction pattern. The step size and the scan speed were 0.05° (2θ) and 5°/min, respectively. For these set of conditions, the X-ray beam passes a sufficiently long distance through the coating to provide the observed diffraction patterns. Surface imaging analysis was performed using a high-performance and ultra high resolution scanning electron microscope (Hitachi S-4800). The secondary electron imaging was performed on W−Ti−O films grown on Si wafers using carbon paste at the ends to avoid charging problems.

The optical properties and surface/interface characteristics were probed by spectroscopic ellipsometry (SE). The measurements were made using a W. A. Woollam VVASE spectroscopic ellipsometer operating in the wavelength range of 250−1350 nm with a step size of 2 nm and at angles of incidence of 65°, 70°, and 75°, near the Brewster's angle of silicon. Number of revolutions per measure was set at 20. The ellipsometry data analysis was performed using commercially available WVASE32 software.[58]

In addition to ellipsometry measurements, spectrophotometric measurements were also employed to probe the transparent nature and band gap analysis of the W−Ti−O films. Spectrophotometric measurements were made using a Cary 5000 UV−vis-NIR double-beam spectrophotometer. W−Ti−O films grown on optical grade quartz were employed for these measurements. The quartz substrates employed extends the transparency range down to ∼190 nm and determines the absorption edge extending into the ultraviolet (UV) region, which is more than sufficient to determine the band gap shift in deficient or stoichiometric or metal incorporated WO_3 films, specifically the Ti-doped tungsten oxide films in this case.

III. OPTICAL MODEL AND THEORY

Optical constants of the Ti-doped WO_3 films were primarily probed by SE, which measures the relative changes in the amplitude and phase of the linearly polarized monochromatic incident light upon oblique reflection from the sample surface. The experimental parameters obtained by SE are the angles Ψ (azimuth) and Δ (phase change), which are related to the microstructure and optical properties, defined by[59−62]

$$\rho = R_p/R_s = \tan\Psi \exp(i\Delta) \tag{1}$$

where R_p and R_s are the complex reflection coefficients of the light polarized parallel and perpendicular to the plane of incidence, respectively. The spectral dependencies of ellipsometric parameters Ψ (azimuth) and Δ (phase change) can be fitted with appropriate models to extract film thickness and the optical constants, i.e., the refractive index (n) and extinction coefficient (k), based on the best fit between experimental and simulated spectra.[59,60] In the present case, the Levenberg-Marquardt regression algorithm was used for minimizing the mean-squared error (MSE):[59]

$$\mathrm{MSE} = \frac{1}{2N - M}\sum_{i=1}^{n}\left[\left\{\frac{(\Psi_{\mathrm{exp}} - \Psi_{\mathrm{calc}})}{\sigma_{\Psi i}^{\mathrm{exp}}}\right\}^2 + \left\{\frac{(\Delta_{\mathrm{exp}} - \Delta_{\mathrm{calc}})}{\sigma_{\Delta i}^{\mathrm{exp}}}\right\}^2\right] \tag{2}$$

where Ψ_{exp}, Ψ_{calc} and Δ_{exp}, Δ_{calc} are the measured (experimental) and calculated ellipsometry functions, N is the number of measured Ψ, Δ pairs, M is the number of fitted parameters in the optical model, and σ are standard deviations of the experimental data points.

Extracting meaningful physical information from ellipsometry requires the construction of an optical model of the sample which generally accounts a number of distinct layers with individual optical dispersions. Interfaces between these layers are optical boundaries at which light is refracted and reflected according to the Fresnel relations. The stack model used to simulate the spectra purpose of determining the optical constants of Ti-doped WO_3 films is schematically shown in Figure 1. The model contains, from top, Ti-doped WO_3 film, SiO_2 interface, and Si substrate. The surface and interface roughness were also considered in order to accurately fit the

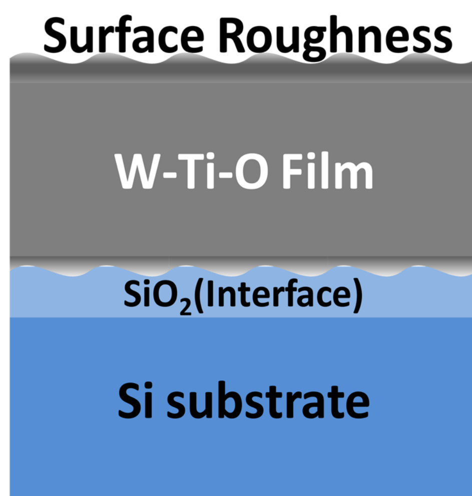

Figure 1. Stack model of the sample constructed for ellipsometry data analysis.

experimental data. The Tauc–Lorentz (TL) model was used and empirical parametrization is based on the Tauc expression for the imaginary part (ε_2) of the dielectric function.[45] For a single transition, the complex dielectric function ε_2 is defined as[59]

$$\varepsilon_2(E) = \left[\frac{A_L E_0 C(E - E_g)^2}{(E^2 - E_o{}^2)^2 + C^2E^2}\cdot\frac{1}{E}\right] \tag{3}$$

where E_0 is the resonance energy, E_g represents band gap energy, E photon energy, and A_L and C are the amplitude and broadening coefficient of the ε_2 peak, respectively, The aforementioned model allowed for the determination of the optical constants, n and k, as well as thickness verification. Note that the real and imaginary parts of the dielectric function are related to n and k as $\varepsilon_1 = n^2 - k^2$; $\varepsilon_2 = 2nk$.

IV. RESULTS AND DISCUSSION

The scanning electron microscopy (SEM) images of W–Ti–O films grown at various T_s are shown in Figure 2. The SEM images did not reveal the presence of any crystalline particles. The SEM cross-sectional images of the representative W–Ti–O films are shown in Figure 3. Images shown are obtained for W–Ti–O films grown at 400 and 500 °C in upper and upper panels, respectively. The Si-substrate and W–Ti–O film regions are as indicated in the micrographs. Two important observations that can be made from these micrographs are the following. No evidence of significant reaction with the Si-substrate at the interface for W–Ti–O samples grown at T_s = RT − 500 °C is the first. This observation indicates that the W–Ti–O films are stable with the Si substrate within the given set of conditions employed in this work. The later is the film thickness, which can be compared and can be used to validate the data obtained from SE modeling as discussed later in this section.

The crystal structure of the grown films was examined by grazing incidence X-ray diffraction (GIXRD) analyses. The GIXRD patterns of W–Ti–O films grown at various T_s are shown in Figure 4. With the absence of diffraction peaks in GIXRD patterns and no evidence of even nanoparticles in the high-resolution SEM images (Figure 2), it can concluded that the films are completely amorphous. The effect may be due to

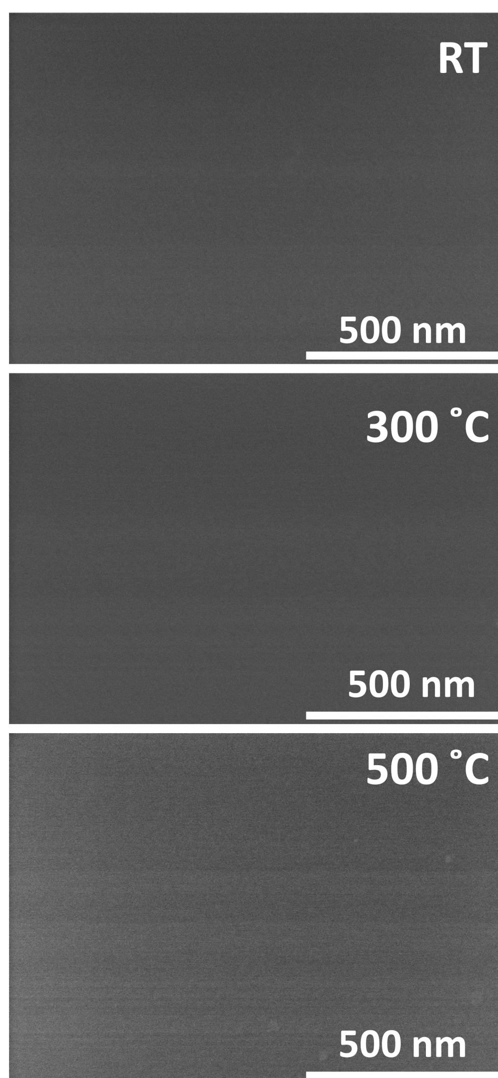

Figure 2. SEM images of W–Ti–O films grown at various temperatures. The images confirm the absence of any particles or crystallites indicating the amorphous nature of the films.

higher concentration of Ti. Our earlier efforts indicated that the pure WO_3 films crystallize in monoclinic structure at T_s = 100–200 °C and tetragonal structure above T_s = 300 °C.[56] Therefore, the result obtained in the present work indicates that the doping of Ti into WO_3 prevents the crystallization and thus induces the amorphous nature. The chemical analyses (not shown) indicate that the effective incorporation of Ti in the films is slightly lower than that of the target. Instead of 80:20 ratio of W/Ti = 80:20 in the bulk of the target, W/Ti ≈ 80:15 was found in the films. The relative difference in the sputtering rates of the elements under the sputtering and reactive gas pressure can account for the observed variation.

Having established the amorphous nature of the grown W–Ti–O films, the attention is now to demonstrate their transparent nature. The optical transmittance spectra of W–Ti–O films are shown in Figure 5. The differences in the spectral transmission curves is due to interference in W–Ti–O films. The spectral transmission curves reveal that the W–Ti–O films in general show a high transparency in the spectral region except where the incident radiation is absorbed across the band gap (E_g). This observation indicates the high-quality and transparent nature of W–Ti–O films. No evident

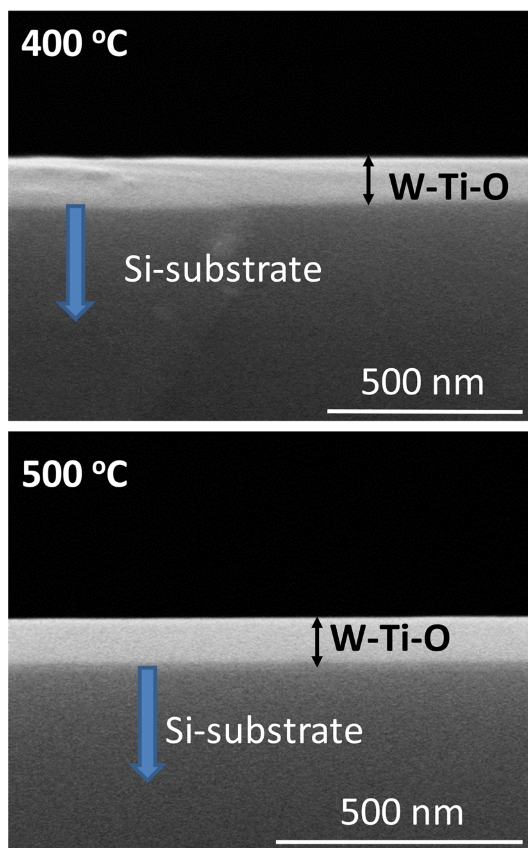

Figure 3. Cross-sectional SEM images of representative W−Ti−O films. The images shown in the upper and lower panel are samples grown at 400 and 500 °C, respectively. The film and substrate regions are as indicated.

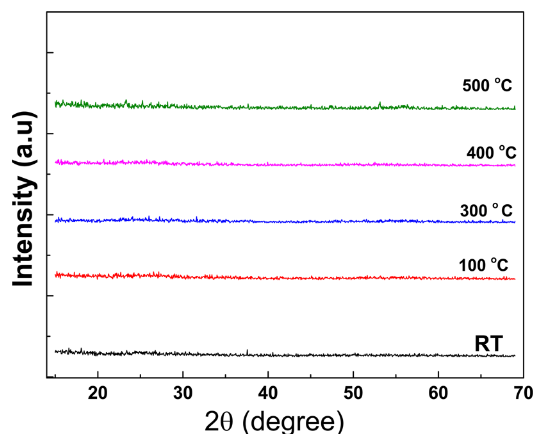

Figure 4. GIXRD patterns of W−Ti−O films grown at various temperatures. The patterns confirm the absence of any diffraction peaks indicating the characteristic amorphous nature of the films grown at all temperatures.

absorption edge shift is noted for W−Ti−O films indicating that there is no significant change in the band gap of the materials fabricated. Optical absorption coefficient and band gap of the W−Ti−O films can be obtained from the spectra shown in Figure 5. The optical absorption coefficient, α, of the films is evaluated using the relation:[56,63,64]

$$\alpha = [1/t]\ln[T/(1-R)^2] \qquad (4)$$

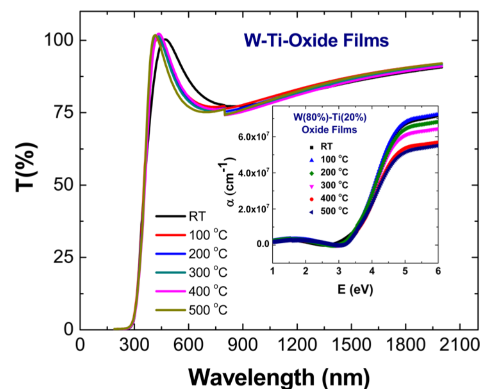

Figure 5. Spectral transmittance characteristics of W−Ti−O films as a function of T_s. Inset shows the optical absorption coefficient of W−Ti−O films.

where T is the transmittance, R the reflectance, and t the film thickness. The average film thickness values determined from both SEM and SE data were employed to obtain the optical absorption coefficient of W−Ti−O films. Also, for transparent films, the R^2 values are extremely small and can be safely neglected to obtain α values. The inset of Figure 5 shows the variation of the optical absorption coefficient of W−Ti−O films grown at various T_s. It is well-known that the optical absorption below E_g follows an exponential behavior.[1,5,56] The absorption, therefore, is exponentially dependent on the energy ($h\nu$) of incident photon in that region. For WO_3, in the E_g region (high absorption) or above the fundamental absorption edge, the absorption follows a power law of the form:[1,5,56,64]

$$(\alpha h\nu) = B(h\nu - E_g)^2 \qquad (5)$$

where $h\nu$ is the energy of the incident photon, α the absorption coefficient, B the absorption edge width parameter, and E_g the band gap. Since the Ti is a dopant and the host-matrix is mainly WO_3, the same analysis has been carried out for the optical data of W−Ti−O films. The absorption data and the plots obtained for W−Ti−O films are shown in Figure 6. It is evident that $(\alpha h\nu)^{1/2}$ vs $h\nu$ results in linear plots in the high absorption region suggesting indirect allowed transitions across E_g of W−Ti−O films. Regression analysis and extrapolating the linear region of the plot to $h\nu$ = 0 provide the band gap value as indicated with an arrow in Figure 6. The E_g obtained for W−Ti−O films is ~3.1 (±0.05) eV, which is almost constant for all

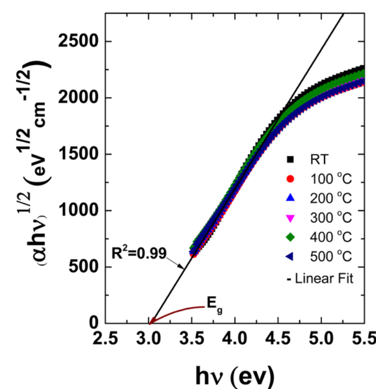

Figure 6. $(\alpha h\nu)^{1/2}$ vs $h\nu$ plots for amorphous W−Ti−O films grown at various substrate temperatures. Extrapolating the linear region of the plot to $h\nu$ = 0 provide the band gap value as indicated with an arrow.

the films. While no effect of T_s on the band gap can be due to the fact all the W−Ti−O films are amorphous, the band gap energy agrees well with that reported for sputter-deposited amorphous WO_3 films.[56]

Finally, we now consider the optical constants of Ti-doped WO_3 films probed by SE. The spectral dependencies of the ellipsometric parameters, Ψ and Δ, determined for Ti-doped WO_3 films grown at various temperatures are shown in Figure 7. The spectral dependencies of ellipsometric parameters Ψ (azimuth) and Δ (phase change) are fitted with appropriate models (discussed in section III) to extract film thickness and the optical constants, i.e., the refractive index (n) and extinction coefficient (k), based on the best fit between experimental and simulated spectra.[59,60] The curves obtained for Ti-doped WO_3 films indicate (Figure 7) a reasonable agreement between the experimental and simulation data.

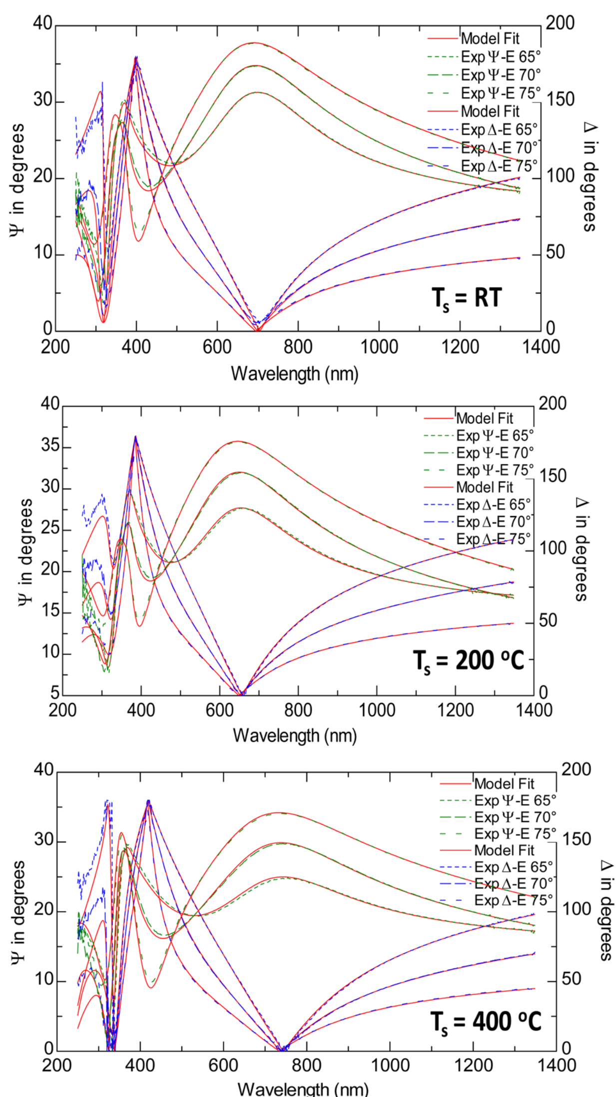

Figure 7. Spectral dependence of Ψ and Δ for Ti-doped WO_3 films grown at various temperatures. The experimental data obtained and modeling curves are shown.

Considering the optical model (stack model shown in Figure 1), the set of W−Ti−O films were modeled with Tauc−Lorentz (TL) oscillators. Furthermore, the pole magnitude, the E_1 (ε_1) offset constant, and the thickness of the film were fitted, as well as the parameters associated with the individual oscillators employed, simultaneously while attempting to locate the best fit for the data by minimizing the MSE. The modeling parameters are listed in Table 1. The governing oscillator of the genosc layer, the TL oscillator has 4 unique parameters associated with it and they are the amplitude (A_L) of the ε_2 peak, the half width (C) of the ε_2 peak, fixed center energy (E_0) of the TL peak, and the Tauc gap (E_g) of amorphous materials. This particular model employed for the set of titanium doped WO_3 amorphous films has been proven effective, in the literature, to model reasonably transparent conducting oxides.[60,65−67] Furthermore, it should be noted that the E_g values obtained from SE analysis and documented in Table 1 are in excellent agreement with that obtained from the analysis of spectrophotometry data for transparent, amorphous W−Ti−O films.

The microstructure information, specifically, film thickness and interfacial oxide thickness of Ti-doped WO_3 films were also determined from SE analysis. The variation of film thickness as a function of growth temperature is shown in Figure 8. It is evident that the film thickness is more or less constant with increasing growth temperature. Most important is that the interfacial oxide (SiO_2) is limited to 2−3 nm at the interface. This result was consistent with our earlier reports for pure WO_3 films, where there was no significant interfacial oxide growth.[68] Inset of Figure 8 shows the variation of surface roughness of the Ti-doped WO_3 films determined from SE analysis. The roughness as determined from SE analysis is very low (<1 nm) for films grown at temperatures 25−100 °C and are not included. To validate the SE analysis and microstructure, the film thickness values obtained from cross-sectional SEM values are also plotted in Figure 8. It can be seen that the film thickness obtained from SE and X-SEM are in good agreement with each other for all the amorphous W−Ti−O films. This observation indicates that the model(s) and SE analysis adopted can reasonably simulate the microstructure and, hence, optical properties of the sputter-deposited W−Ti−O amorphous films.

The spectral dependence of the extinction coefficient (k) determined from SE data for Ti-doped WO_3 films is shown in Figure 9. It is evident that the extinction coefficient values are low and very close to zero in most parts of the spectrum (Figure 9) which indicates very low optical losses due to absorption. The onset or sharp increase in k at short wavelengths is due to the fundamental absorption across the band gap. An understanding of the structural quality of Ti-doped WO_3 films can also be derived from the dispersion profiles of $k(\lambda)$. Specifically, the curves (Figure 8) indicate that the k value of the Ti-doped WO_3 films is almost zero in the visible and near-infrared spectral regions, while for photon energies toward the ultraviolet region, the extinction coefficient increases sharply. The $k(\lambda)$ behavior is obviously related to the optical quality of the films. Strong absorption with no weak shoulders or tailing behavior for the Ti-doped WO_3 films can be attributed to the high quality of the grown layers with a very high transparency, which is also confirmed by the spectrophotometry analysis of films shown above (Figure 5).

The dispersion profiles of index of refraction (n) determined from SE data for Ti-doped WO_3 films are shown in Figure 10. The results indicate a similar behavior as noted in k curves. The "n" dispersion curves also indicate a sharp increase at shorter wavelengths corresponding to fundamental absorption of energy across the band gap. However, the effect of growth

Table 1. Ellipsometry Modelling Parameters of W−Ti−O Films

temperature (°C)	RT	200	300	400	500
Modeling Parameters					
Pole Mag.	8.7786 ± 8.8	481.04 ± 49	525.03 ± 26.2	997.15 ± 152	8.948 ± 10.2
E_1 offset	2.0605 ± 0.0994	−0.92686 ± 0.364	−1.1766 ± 0.188	−4.804 ± 2.89	3.151 ± 29.8
Oscillator 1	Tauc−Lorentz	Tauc−Lorentz	Tauc−Lorentz	Tauc−Lorentz	Tauc−Lorentz
A_L	166.02 ± 8.31	115.67 ± 6.9	114.05 ± 4.15	78.854 ± 4.49	137.49 ± 15.6
E_0	4.0422 ± 0.0139	4.0373 ± 0.0139	4.0422 ± 0.0139	4.0237 ± 0.0165	3.9421 ± 0.0332
C	2.3934 ± 0.109	1.368 ± 0.0417	1.368 ± 0.417	1.0462 ± 0.0439	1.297 ± 0.125
E_g	3.2439 ± 0.00865	3.1687 ± 0.0851	3.1687 ± 0.0085	3.142 ± 0.0168	3.2127 ± 0.0166

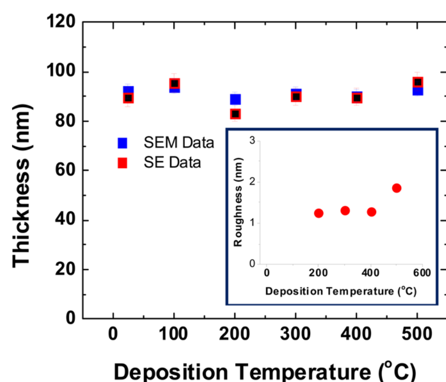

Figure 8. Thickness of Ti-doped WO_3 films grown at various temperatures. Insert shows the variation of surface roughness of the films with growth temperature.

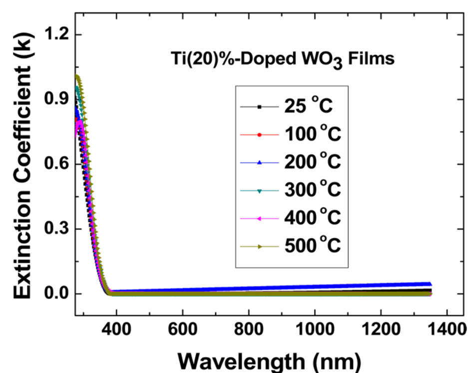

Figure 9. $k(\lambda)$ curves of Ti(20%)-doped WO_3 films grown at various temperatures. The extremely low values of k at λ > 400 nm can be attributed to the transparent nature.

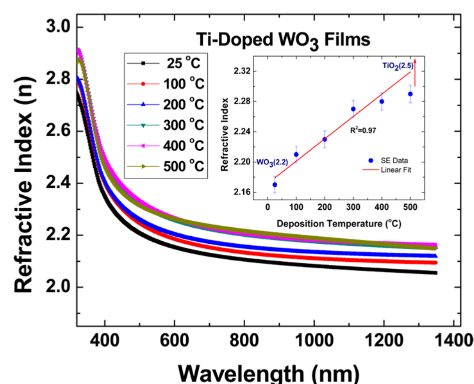

Figure 10. Dispersion profiles of index refraction of Ti(20%)-doped WO_3 films grown at various temperatures. The sharp increase in the index of refraction at $\lambda \leq 400$ nm is due to fundamental absorption across the band gap of the films. Inset shows the functional dependence of index of refraction measured at $\lambda = 550$ nm on the growth temperature of Ti(20%)-doped WO_3 films. The data is compared with that of pure WO_3 and TiO_2. A gradual increase in index of refraction suggests improved packing density of the films with increasing growth temperature.

temperature is evident in the dispersion curves (Figure 10), where there is an increase in "n" values with increasing temperature.

In order to understand the chemistry and physics of Ti-doped WO_3 films and the effect of growth temperature on their optical constants, the refractive index variation of the films at $\lambda = 550$ nm with growth temperature is shown in the inset of Figure 10. The "n" values of the bulk WO_3 and TiO_2 are as indicated in Figure 10. At a $\lambda = 550$ nm, the "n" values increase from 2.17 to 2.31 with increasing growth temperature from 25 to 500 °C. For comparison, at 550 nm, the "n" values of bulk, crystalline WO_3[1,69] and TiO_2[70] are 2.2 and 2.5, respectively. It can be seen (inset, Figure 10) that the data fits a linear dependence on growth temperature indicating the effect of temperature in enhancing the refractive index of Ti-doped WO_3 films. However, it appears that the index of refraction of amorphous W−Ti−O films grown in the temperature range of 400−500 °C is saturated as it is almost constant with a nominal increase. This is evident in both the dispersion curves and the specific "n" values at $\lambda = 550$ nm. Further improvement or changes may be possible only if the film is fully crystallized or if a structural transformation occurs.

A simple model can be formulated to explain the observed functional relationship between the optical constants and growth conditions in Ti-doped WO_3 films. Evident from the results, the dispersion of optical constants depend on the growth temperature. XRD measurements demonstrated that the Ti-doped WO_3 films grown at 25−500 °C are completely amorphous. The observed increase in n values when Ti-doped WO_3 films are grown at higher temperatures can be attributed to the improved packing density of the films. However, we believe that the packing density slightly improves but not significantly. Perhaps, the temperature is not enough to promote the structural order but is sufficient to increase the mobility of ad-atoms to join together to increase the packing density of the materials in the films leading to observed increase in "n" values. In order to confirm the validity of this, the relative density (which is the ratio of film density to that bulk of the material) Ti-doped WO_3 films can be approximated from the Lorentz−Lorentz relation[71] using the measured index of refraction values. The functional dependence of the relative density of Ti-doped WO_3 films on the growth temperature is shown in Figure 11. It can be seen that there is a direct

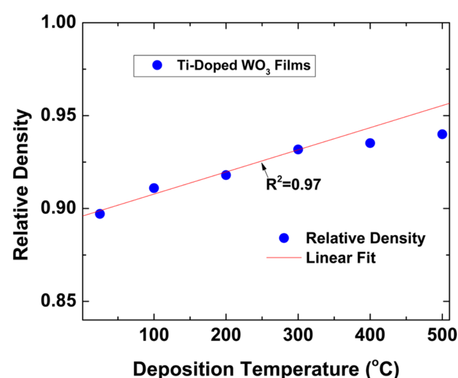

Figure 11. Functional dependence of relative density of the Ti(20%)-doped WO_3 films on the growth temperature. The relative density values were calculated from the Lorentz–Lorentz model.

correlation between the index of refraction, relative density, and growth temperature suggesting that the improved packing density accounts for the observed optical constants and their behavior in Ti-doped WO_3 films.

V. CONCLUSIONS

Ti-doped WO_3 films were fabricated using sputter-deposition by varying deposition temperature in the range of 25–500 °C. The structure and optical properties of the grown W–Ti–O films were evaluated as a function of growth temperature. Crystal structure and surface morphology analyses using GIXRD and SEM, respectively, confirm that Ti-doped WO_3 films were amorphous at all growth temperatures. The effect Ti-incorporation and associated amorphization is dominant in the entire range (25–500 °C) of growth temperatures. Spectrophotometry analyses indicate that grown W–Ti–O films are transparent in nature. Optical constants and a correlation between growth temperature and optical property of the grown films were evaluated using spectroscopic ellipsometry. The stack model containing, from top, Ti-doped WO_3 film, SiO_2 interface, and Si substrate coupled with the Tauc–Lorentz model, where empirical parametrization is based on the Tauc expression for the imaginary part (ε_2) of the dielectric function, reasonably simulates the microstructure and optical properties of the grown W–Ti–O films. The results indicate that the Ti-doped WO_3 films grown at T_s = 25–500 °C are highly transparent and exhibit low optical losses in the visible and near-infrared regions. A correlation between the energy absorption and associated transitions is noted in spectrohotometry and SE analyses confirming the validity of optical behavior of the W–Ti–O films derived from both methods. While there is no significant improvement in the structural order noted, the SE data indicate that the index of refraction of the samples increases from 2.17 to 2.31 with increasing growth temperature from 25 to 500 °C. The increased packing density in the films with increasing temperature is attributed to the linear trend observed in the index of refraction.

AUTHOR INFORMATION

Corresponding Author

*E-mail: rvchintalapalle@utep.edu.

Notes

The authors declare no competing financial interest.

ACKNOWLEDGMENTS

This work is supported by the National Science Foundation (NSF) with NSF-PREM Grant No. DMR-1205302. The Hitachi 4800 SEM used for the morphology and X-ray chemical analysis of the samples in this work was acquired through the support from NSF (Grant NSF-DMR-0521650).

REFERENCES

(1) Granqvist, C. G. *Handbook of Inorganic Electrochromic Materials*; Elsevier: New York, 1995; pp 5–7.
(2) Zhang, Y.; Lee, S. H.; Mascarenha, A.; Deb, S. K. *Appl. Phys. Lett.* **2008**, *93*, 203508–203508-2.
(3) Ramana, C. V.; Utsunomiya, S.; Ewing, R. C.; Julien, C. M.; Becker, U. *J. Phys. Chem. B* **2006**, *110*, 10430–10435.
(4) Berggren, L.; Jonsson, J. C.; Niklasson, G. A. *J. Appl. Phys.* **2007**, *102*, 083538–083538–7.
(5) Lin, Y. S.; Chen, H. T.; Lai, J. Y. *Thin Solid Films* **2009**, *518*, 1377–1381.
(6) Lu, D.; Chen, J.; Chen, H. J.; Gong, J.; Deng, S. Z.; Xu, N. S.; Liu, Y. L. *Appl. Phys. Lett.* **2007**, *90*, 041919–041919-3.
(7) Lee, D. S.; Han, S. D.; Lee, D. D. *Sens. Actuators, B* **1999**, *60*, 57–63.
(8) Baeck, S. H.; Jaramillo, T.; Stucky, G. D.; McFarland, E. W. *Nano Lett.* **2002**, *2*, 831–834.
(9) Lee, D. S.; Nam, K. H.; Lee, D. D. *Thin Solid Films* **2000**, *375*, 142–146.
(10) Wang, L.; Teleki, S. E.; Pratsinis, S. E.; Gouma, P. I. *Chem. Mater.* **2008**, *20*, 4794–4796.
(11) Kawasaki, H.; Namba, J.; Iwatsuji, K.; Suda, Y.; Wada, K.; Ebihara, K.; Ohshima. *Appl. Surf. Sci.* **2002**, *197–198*, 547–551.
(12) Ionescu, R.; Llobet, E.; Brezmes, J.; Vilanova, X.; Correig, X. *Sens. Actuators, B* **2003**, *95*, 177–182.
(13) Moulzolf, S. C.; Ding, S.; Lad, R. J. *Sens. Actuators, B* **2001**, *77*, 375–382.
(14) Satnkova, M.; Vilanova, X.; Llobet, E.; Calderer, J.; Bittencourt, C.; Pireaux, J. J.; Correig, X. *Sens. Actuators, B* **2005**, *105*, 271–277.
(15) Xie, G.; Yu, J.; Chen, X.; Jiang, Y. *Sens. Actuators, B* **2007**, *123*, 909–914.
(16) Santucci, S.; Cantalini, C.; Crivellari, M.; Lozzi, L.; Ottaviano, L.; Passacantanso, M. J. *J. Vac. Sci. Technol. A* **2000**, *18*, 1077–1082.
(17) Gouma, P. I.; Kalyanasundaram, K. *Appl. Phys. Lett.* **2008**, *93*, 244102–244102-3.
(18) Huelser, T. P.; Lorke, A.; Ifeacho, P.; Wiggers, H.; Schulz, C. J. *J. Appl. Phys.* **2007**, *102*, 124305–124305–7.
(19) Marsen, B.; Miller, E. L.; Paluselli, D.; Rocheleau, R. E. *Int. J. Hydrogen Energy* **2008**, *32*, 3110–3115.
(20) Paluselli, D.; Marsen, B.; Miller, E. L.; Rocheleau, R. E. *Electrochem. Solid-State Lett.* **2005**, *8*, G301–G303.
(21) Sun, Y.; Murphy, C. J.; Reyes-Gil, K. R.; Reyes-Garcia, E. A.; Thornton, J. M.; Morris, N. A.; Raftery, D. *Int. J. Hydrogen Energy* **2004**, *34*, 8476–8484.
(22) Zheng, H.; Tachibana, Y.; Kalantar-Zadeh, K. *Langmuir* **2010**, *26*, 19148–19152.
(23) Zheng, H.; Ou, J. Z.; Strano, M. S.; Kaner, R. B.; Mitchell, A.; Kalantar-Zadeh, K. *Adv. Funct. Mater.* **2011**, *21*, 2175–2196.
(24) Ou, J. Z.; Balendhran, S.; Field, M. R.; McCulloch, D. G.; Zoolfakar, A. S.; Rani, R. A.; Zhuiykov, S.; O'Mullane, A. P.; Kalantar-Zadeh, K. *Nanoscale* **2012**, *4*, 5980–5988.
(25) Waller, M. R.; Townsend, K. T.; Zhao, J.; Sabio, E. M.; Chamousis, R. L.; Browning, N. D.; Osterloh, F. E. *Chem. Mater.* **2012**, *24*, 698–704.
(26) Wang, S. J.; Lu, W. J.; Cheng, G.; Cheng, K.; Jiang, X. H. *Appl. Phys. Lett.* **2009**, *94*, 263106–263106-3.
(27) Ha, J. H.; Muralidharan, P.; Kim, D. K. *J. Alloys Compd.* **2009**, *475*, 446–451.
(28) Zhang, J.; Tu, J.; Xia, X.; Wang, X.; Gu, C. *J. Mater. Chem.* **2011**, *21*, 5492–5498.

(29) Jiao, Z.; Sun, X. W.; Wang, J.; Ke, L.; Demir, H. V. *J. Phys. D: Appl. Phys.* **2010**, *43*, 285501−285501-6.
(30) Wang, J.; Khoo, E.; Lee, P. S.; Ma, J. *J. Phys. Chem.* **2008**, *112*, 14306−14312.
(31) Ma, D.; Shi, G.; Wang, H.; Zhang, Q.; Li, Y. *J. Mater. Chem. A* **2013**, *1*, 684−691.
(32) Phuruangrat, A.; Ham, D. J.; Hong, S. J.; Thongtem, S.; Lee, J. S. *J. Mater. Chem.* **2010**, *20*, 1683−1690.
(33) Su, J.; Feng, X.; Sloppy, J. D.; Guo, L.; Grimes, C. A. *Nano Lett.* **2011**, *11*, 203−208.
(34) Li, L.; Zhang, Y.; Fang, X.; Zhai, T.; Liao, M.; Sun, X.; Koide, Y.; Bando, Y.; Golberg, D. *J. Mater. Chem.* **2011**, *21*, 6525−6530.
(35) Lai, C. W.; Sreekantan, S. *Int. J. Hydrogen Energy* **2013**, *38*, 2156−2166.
(36) Kwong, W. L.; Savvides, N.; Sorrell, C. C. *Electrochim. Acta* **2012**, *75*, 371−380.
(37) Vidyarthi, V. S.; Hofmann, M.; Savan, A.; Sliozberg, K.; Konig, D.; Beranek, R.; Schuhmann, W.; Ludwig, A. *Int. J. Hydrogen Energy* **2011**, *36*, 4724−4731.
(38) Santato, C.; Odziemkowski, M.; Ulmann, M.; Augustynski, J. *J. Am. Chem. Soc.* **2001**, *123*, 10639−10649.
(39) Kirchgeorg, R.; Berger, S.; Schmuki, P. *Chem. Commun.* **2011**, *47*, 1000−1002.
(40) Chen, H. J.; Xu, N. S.; Deng, S. Z.; Lu, D. Y.; Li, Z. L.; Zhou, J.; Chen, J. *Nanotechnology* **2007**, *18*, 205701.
(41) Jerman, M.; Mergel, D. *Thin Solid Films* **2007**, *515*, 6904−6908.
(42) Jerman, M.; Qiao, Z.; Mergel, D. *Appl. Opt.* **2005**, *44*, 3006−3012.
(43) Mergel, D. *Thin Solid Films* **2001**, *397*, 216−222.
(44) Mahanthi, M.; Ghosh, T.; Basak, D. *Nanoscale* **2011**, *3*, 4427−4433.
(45) Xieo, M. W.; Wang, L. S.; Huang, X. J.; Wu, Y. D.; Dang, Z. *J. Alloys Compd.* **2009**, *470*, 486−491.
(46) Hong Pan, J.; Lee, W. I. *Chem. Mater.* **2006**, *18*, 847−853.
(47) Keller, V.; Bernhardt, P.; Garin, F. *J. Catal.* **2003**, *215*, 129−138.
(48) Kobayashi, M.; Miyoshi, K. *Appl. Catal., B* **2007**, *72*, 253−261.
(49) Higashimoto, S.; Sakiyama, M.; Azuma, M. *Thin Solid Films* **2006**, *503*, 201−206.
(50) Smith, W.; Zhao, Y. *J. Phys. Chem. C* **2008**, *112*, 19635−19641.
(51) Smith, W.; Wolcott, A.; Fitzmorris, R. C.; Zhang, J. Z.; Zhao, Y. *J. Mater. Chem.* **2011**, *21*, 10792−10800.
(52) Ferroni, M.; Boscarino, D.; Comini, E.; Gnani, D.; Guidi, V.; Martinelli, G.; Nelli, P.; Rigato, V.; Sberveglieri, G. *Sens. Actuators, B* **1999**, *58*, 289−294.
(53) Gerlich, M.; Kornely, S.; Fleischer, M.; Mixner, H.; Kassing, R. *Sens. Actuators, B* **2003**, *93*, 503−508.
(54) Kalidindi, N. R.; Manciu, F. S.; Ramana, C. V. *ACS Appl. Mater. Interfaces* **2011**, *3*, 863−868.
(55) Kalidindi, N. R.; Kamala Bharathi, K.; Ramana, C. V. *Appl. Phys. Lett.* **2010**, *97*, 142107−142107-3.
(56) Gullapalli, S. K.; Vemuri, R. S.; Ramana, C. V. *Appl. Phys. Lett.* **2010**, *96*, 171903−171903-3.
(57) Vemuri, R. S.; Kamala Bharathi, K.; Gullapalli, S. K.; Ramana, C. V. *ACS Appl. Mater. Interfaces* **2010**, *2*, 2623−2628.
(58) *Guide to Using WVASE32 Spectroscopic Ellipsomtry Data Acquisition and Analysis Software*; J. A. Woollam Co., Inc.: Lincoln, NE, 2008.
(59) Jellison, G. E., Jr. *Thin Solid Films* **1996**, *290−291*, 40−45.
(60) Fujiwara, H. *Spectroscopic Ellipsometry: Principles and Applications*; John Wiley & Sons Inc.: Chichester, U.K., 2007; pp147−265.
(61) Ramana, C. V.; Utsunomiya, S.; Ewing, R. C.; Becker, U.; Atuchin, V. V.; Aliev, V.Sh.; Kruchinin, V. N. *Appl. Phys. Lett.* **2008**, *92*, 011917−011917-3.
(62) Mudavakkat, V. H.; Atuchin, V. V.; Kruchinin, V. N.; Kayani, A.; Ramana, C. V. *Opt. Mater.* **2012**, *34*, 893−900.
(63) Tyagi, P.; Vedeshwar, A. G. *Phys. Rev. B* **2002**, *66*, 075422.
(64) Vemuri, R. S.; Engelhard, M. H.; Ramana, C. V. *ACS Appl. Mater. Interfaces* **2012**, *4*, 1371−1377.
(65) Tauc, J.; Grigorovici, R.; Vancu, A. *Phys. Status Solidi B* **1966**, *15*, 627−637.
(66) Rovira, P. I.; Collins, R. W. *J. Appl. Phys.* **1999**, *85*, 2015−2015-11.
(67) Fujiwara, H.; Kondo, M. *Phys. Rev. B* **2005**, *71*, 075109−075109−10.
(68) Manciu, F. S.; Enriquez, J. L.; Durrer, W. G.; Yun, Y.; Ramana, C. V.; Gullapalli, S. K. *J. Mater. Res.* **2010**, *25*, 2401−2404.
(69) Hong, K.; Kim, K.; Kim, S.; Lee, I.; Cho, H.; Yoo, S.; Choi, H. W.; Lee, N.-Y.; Tak, Y.-H.; Lee, J.-L. *J. Phys. Chem. C* **2011**, *115*, 3435.
(70) Diebold, U. *Surf. Sci. Rep.* **2003**, *48*, 53−229.
(71) Born, M. and Wolf, E. In *Principles of Optics*, 7th ed.; Cambridge University Press: Cambridge, U.K., 1999; p98.